Interlayer excitonic superfluidity in graphene

D. S. L. Abergel,[1] M. Rodriguez-Vega,[2] Enrico Rossi,[2] and S. Das Sarma[1]

[1]*Condensed Matter Theory Center, University of Maryland, College Park, Maryland 20742, USA*

[2]*Department of Physics, College of William and Mary, Williamsburg, Virginia 23187, USA*

We discuss the conditions under which the predicted (but not yet observed) zero-field inter-layer excitonic condensation in double layer graphene has a critical temperature high enough to allow detection. Crucially, disorder arising from charged impurities and corrugation in the lattice structure—invariably present in all real samples—affects the formation of the condensate via the induced charge inhomogeneity. In the former case, we use a numerical Thomas-Fermi-Dirac theory to describe the local fluctuations in the electronic density in double layer graphene devices and estimate the effect these realistic fluctuations have on the formation of the condensate. To make this estimate, we calculate the critical temperature for the interlayer excitonic superfluid transition within the mean-field BCS theory for both optimistic (unscreened) and conservative (statically screened) approximations for the screening of the interlayer Coulomb interaction. We also estimate the effect of allowing dynamic contributions to the interlayer screening. We then conduct similar calculations for double quadratic bilayer graphene, showing that the quadratic nature of the low-energy bands produces pairing with critical temperature of the same order of magnitude as the linear bands of double monolayer graphene.

PACS number(s): 73.22.Pr, 74.62.En, 67.85.Jk, 71.35.−y

I. INTRODUCTION

The prediction of an interlayer direct Coulomb interaction driven room-temperature excitonic condensate at zero magnetic field in double monolayer graphene[1,2] (DMG), double quadratic bilayer graphene[3] (DQBG), and hybrid monolayer-bilayer graphene systems[4] has captured much attention both for the fundamental interest in the existence of a zero-field condensate and for possible applications in devices, including ultrafast switches and dispersionless field-effect transitors.[5] However, despite considerable experimental effort, the condensate has yet to be observed in Coulomb drag experiments in zero magnetic field.[6,7] There are two possible reasons why this is so. First, the critical temperature (T_c) may simply be too small (i.e., much lower than the optimistic mean-field theoretic predictions for ideal systems) and therefore the condensate is destroyed by simple thermal fluctuations. Second, it is possible that disorder in the form of electron-impurity scattering,[8,9] scattering from vacancy sites in the lattice,[10] or from the presence of inhomogeneity in the charge density distribution[11] is suppressing formation of the condensate. In this work, we examine the last of these possibilities. In order to avoid any confusion, we emphasize right at the beginning that we are considering here only the case of interlayer superfluidity in double-layer graphene systems and not the question of superconductivity in individual (i.e., single layer) monolayer graphene and bilayer graphene, which is also an interesting problem and is attracting a lot of attention. These two problems, i.e., the interlayer superfluidity of our interest and superconductivity in individual graphene layers, are completely distinct physical and mathematical problems. In the case of interlayer superfluidity, the individual layers of graphene are not superconducting, only the interlayer Coulomb correlations between the two layers drive the system into an interlayer neutral superfluid. Similar physics, often also referred to as "excitonic condensation," could, in principle, occur in any two-component (double-layer or two bands) electron-hole system if the intercomponent interaction is strong enough.

To address the issue of the critical temperature in the clean limit, it is known that the size of the predicted excitonic gap in DMG depends very strongly on the choice of screening of the interlayer Coulomb interaction.[1,2,12–15] For DMG embedded in a dielectric medium such as hBN or SiO$_2$, in the situation where the two layers have equal chemical potential in opposite bands, and where $k_F d = 0$ (where k_F is the Fermi wave vector and d is the interlayer separation), it is known that the prediction of room-temperature superfluidity is only valid for the unscreened Coulomb interaction approximation.[12] Using static screening in the analysis (replacing the unscreened Coulomb interaction) exponentially suppresses the predicted excitonic gap to a regime where it is unmeasurable.[14,15] A dynamic screening approximation[12] gives a gap that is intermediate between these two. If self-consistent screening of the Coulomb interaction including the gap at the Fermi surface caused by the existence of the condensate is considered with dynamic screening,[12] the superfluid gap sharply increases if the effective interaction parameter $\alpha = e^2/(\epsilon \hbar v_F) \gtrsim 1.5$ (or equivalently $\epsilon < 1.45$, where ϵ is the dielectric constant of the medium and v_F is the Dirac band velocity of monolayer graphene). This self-consistent screening mechanism is also applied in the static screening case[13] where the enhancement in the gap size is found at $\alpha \approx 2.2$, corresponding to $\epsilon = 0.9$, implying all physical values of ϵ are above the threshold. The impact of vertex corrections has also been studied[13] and is claimed to be weak, although they may slightly increase the pairing strength. Interband processes[12,16] have also been shown to slightly increase the critical temperature. In the context of quadratically dispersing bands, room-temperature superfluidity was predicted for electron-hole systems with ordinary parabolic dispersion as early as 1976 by Lozovik and Yudson.[17] The self-consistent screening method was also applied to DQBG[3] where a similar enhancement of the pairing was found at low carrier density (or, equivalently, small values of $k_F d$). However, we believe there are some technical issues with the method of the self-consistent screening calculation, which we explain and discuss in the Appendix—these

technical issues, although important in their own right, are not particularly germane to the issue of charge inhomogeneity, which is the main topic studied in our work.

The role of disorder has also been studied, and it was shown in Refs. [8–10] that intralayer momentum scattering by short-range disorder typically does not reduce T_c substantially. However, long-range disorder in the form of charge inhomogeneity does play a key role[11] because in this case the energy scale to which the disorder must be compared is the excitonic gap, which may be small depending on the choice of screening in the interlayer interaction. The carrier density inhomogeneities induced by the presence of long-range disorder lead to differences in the chemical potential in the two layers that remove the perfect nesting of the Fermi surfaces and therefore strongly suppress T_c. This effect is analogous to the Clogston-Chandrasekhar limit of BCS superconductivity and the associated destruction of the pairing. It must be emphasized that although the usual momentum scattering by disorder does not affect the excitonic condensation by virtue of Anderson's theorem, any density or chemical potential fluctuations between the two layers would act as a random magnetic field for the s-wave superconductor, strongly suppressing the superfluidity. Random charged impurities in the environment invariably lead to interlayer chemical potential fluctuations because of their long-range Coulombic nature. One must therefore carefully distinguish between the disorder-induced momentum scattering (which may not be particularly detrimental to the predicted interlayer superfluidity) and the disorder-induced density inhomogeneity (which is extremely detrimental to the superfluidity). The effects of density imbalance in the BCS-BEC crossover region have also been investigated,[18] but since the interlayer interaction in graphene double layers is relatively weak, our results are located firmly in the BCS regime and the added complexity of the phase diagram near the crossover is not of immediate practical concern.

In this article, in Sec. II, we give a comprehensive description of the conditions under which the condensate should be observable in DMG. To do this, we accomplish two main tasks. First, we describe how T_c behaves in the presence of a finite imbalance in the chemical potentials of the two layers, a calculation which was not previously reported. We estimate T_c for both unscreened and statically screened interlayer interactions as a function of the overall chemical potential ($\bar{\mu}$) and asymmetry in the chemical potential in the two layers ($\delta\mu$), and provide estimates for the dynamic screening case. Our reason for carrying out calculations using both unscreened and statically screened Coulomb interactions is the fact that they respectively represent the most optimistic and the most pessimistic scenarios for the excitonic condensation to occur with the respective T_c estimates for the two approximations differing by several orders of magnitude. Our theory thus provides upper and lower bounds on the expected T_c in the system without getting into the complications of attempting a dynamical screening calculation of T_c in the presence of disorder, which is challenging and beyond the scope of the current work and remains a problem for the future. The main aim is to describe the role of charge inhomogeneity, which we can do within these two well-defined theoretical approximations. We find that any finite $\delta\mu$ has the effect of

reducing T_c, and that when $\delta\mu$ is comparable to the size of the excitonic gap (Δ), T_c becomes zero consistent with the Clogston-Chandrasekhar limit in metallic superconductors. The second task is to provide a comprehensive description of the nature of the charge inhomogeneity in DMG devices. We use Thomas-Fermi-Dirac theory (TFDT)[19] to estimate the spatial fluctuation in $\delta\mu$ induced by randomly placed charged impurities. This is a completely new application of TFDT and nothing similar has previously been attempted to describe double layer graphene systems. In this way, we gain a full understanding of the nature of the correlations in the disorder of the two layers, and obtain quantitatively accurate estimates of the spatial size and magnitude of the charge fluctuations for realistic experimental parameters. We then link the two calculations by assuming that the variance of the disorder-induced potential fluctuations represents the typical mismatch or imbalance of the Fermi energies in the two layers. We find that when charged impurities are located close to the DMG, the fluctuations in $\delta\mu$ have a length scale of the order of 10 nm, and that $\delta\mu \sim \bar{\mu} \gg \Delta$ indicating that the excitonic condensate will not be able to form in this regime, as it is suppressed totally by the disorder induced interlayer chemical potential fluctuations. However, when a clean spacer layer is used to separate the DMG from the SiO_2 where the impurities reside, the fluctuations in $\delta\mu$ reduce by an order of magnitude for comparable impurity densities. In this regime, when the impurity density is low, we find that it is possible for the excitonic condensate to form for reasonable T_c estimates as given by dynamic screening.

In Sec. III, we present the condensate analysis of the DQBG system at the same level of approximation as that of the DMG. This analysis has also not been reported previously. We find that the alteration in the single-particle band structure and chirality properties of the underlying layers in going from DMG to DQBG causes some qualitative change in the evolution of T_c with $\bar{\mu}$ for the unscreened interaction, but that the gap size is quantitatively similar for experimentally pertinent parameters. Crucially, the behavior of T_c with $\delta\mu$ is unchanged. As mentioned above, we believe that there are certain technical issues with the method of the self-consistent screening calculations presented in other works[3,12,13] and we discuss this in the Appendix.

II. DOUBLE MONOLAYER GRAPHENE

A. T_c for asymmetrically doped layers

We begin by describing the role of a finite chemical potential difference between the two layers in reducing T_c. A rigorous estimate of T_c in the nondisordered case is already an intractable calculation since the inclusion of dynamic screening effects in the interlayer interaction demands that the vertex corrections be included in the theory. In fact, there is no Migdal's theorem when considering superconductivity (or fermionic superfluidity) induced by electron-electron interactions, and thus vertex corrections must, in principle, be included in the theory even for the unscreened interaction. As such, all mean-field BCS type theories of interlayer excitonic superfluidity are somewhat suspect strictly from a theoretical viewpoint since vertex corrections are uncritically neglected.

However, in the presence of dynamic screening, the theory becomes particularly suspect if vertex corrections from the ladder diagrams, which contribute to Migdal's theorem, are left out since the interaction itself now is calculated in an approximation including infinite number of electron-hole loops. The role of vertex corrections and other processes which go beyond Migdal's theorem have been discussed in Ref. 20. Therefore, since all analytically approachable calculations will either overestimate (i.e., the unscreened case) or underestimate (i.e., the statically screened case), the actual T_c, we shall show how the chemical potential imbalance will affect the formation of the excitonic condensate for two distinct model calculations. We consider our calculation not to give a quantitative estimate of the real T_c, but to provide a comprehensive survey of the role of disorder in the form of charge inhomogeneity. Using the unscreened interlayer interaction (which will systematically overestimate T_c), and the statically screened interlayer interaction (which will underestimate T_c), we show that when $\delta\mu > 0$ is less than the excitonic gap (which we label Δ), T_c is reduced but remains finite. When $\delta\mu \sim \Delta$, T_c becomes zero. Thus the disorder-induced chemical potential imbalance or asymmetry is a key parameter determining the existence or absence of the excitonic condensation, which needs to be taken into account in the experimental search for interlayer superfluidity.

It is convenient to assume that the upper layer is doped with electrons, the lower layer with holes, and to perform a particle-hole transformation in the lower layer such that both layers are described by a chemical potential with positive sign. We then characterize the system by their average chemical potential $\bar{\mu} = (\mu_u + \mu_l)/2$ and difference $\delta\mu = \mu_u - \mu_l$. This implies that, for a given $\bar{\mu}$, the maximum value of $\delta\mu$ possible is $2\bar{\mu}$. Note that in other works relating to the excitonic condensate in DMG, it was assumed that $\mu_u = \mu_l$ giving perfect nesting of the Fermi surfaces in the two layers.[1–3,8–10,12–17] Within the mean-field theory and the BCS approximation, the temperature-dependent gap function is given by[11]

$$\Delta_{\mathbf{k}}(T) = \sum_{\mathbf{k}'} V(\mathbf{k}' - \mathbf{k}) \frac{\Delta_{\mathbf{k}'}(T) f(\mathbf{k},\mathbf{k}') N(\mathbf{k}',T)}{E_{\mathbf{k}'}}. \quad (1)$$

In this equation, $V(\mathbf{q}) = V(\mathbf{q},0)$ is the static limit of the random phase approximation (RPA) for the interlayer potential, $f(\mathbf{k},\mathbf{k}') = [1 + \cos(\theta_k - \theta_{k'})]/2$ comes from the chirality of electrons in monolayer graphene, $N(\mathbf{k}',T) = n_\beta(\mathbf{k}',T) - n_\alpha(\mathbf{k}',T)$ is the finite temperature occupation factor of the excitonic bands labeled by α and β, which contain $\delta\mu$ and $E_{\mathbf{k}'} = [(v_F k' - \bar{\mu})^2 + \Delta_{\mathbf{k}}^2]^{1/2}$, where v_F is the monolayer graphene Fermi velocity. We identify the excitonic gap Δ as the peak value of this function, which, in the BCS limit, is found at $k = k_F$. We define T_c as the lowest value of T for which the gap function is zero for all k. We find this condition numerically, and it gives a value which is of the same order of the standard prediction $\Delta = 1.76 T_c$ from the textbook constant gap approximation to mean-field theory. Our value for T_c is a little smaller due to the nonconstant gap function and full momentum-dependent interaction, which we retain in the calculation. We note as an aside that in the presence of the Fermi surface mismatch in the two layers (i.e., a chemical potential or density imbalance between the
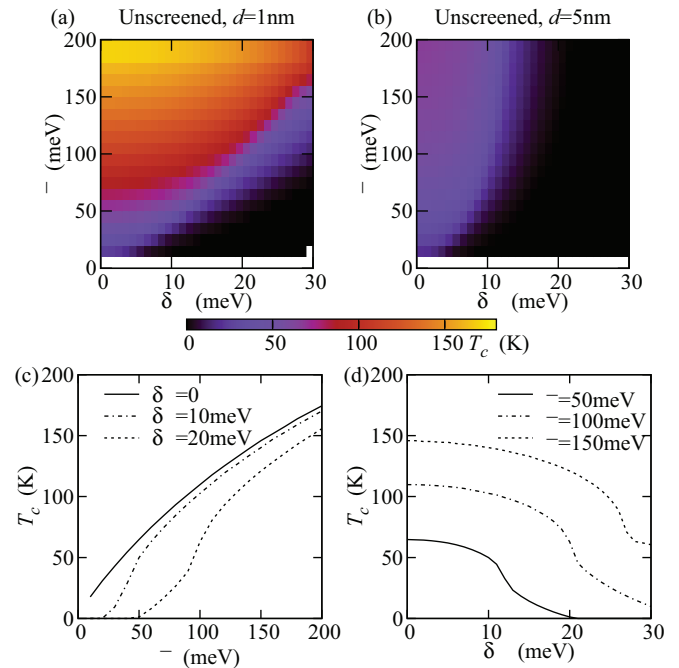

FIG. 1. (Color online) T_c for the unscreened interaction in dielectric environment $\epsilon = 3.9$ (a) and (b) show color plots as a function of $\bar{\mu}$ and $\delta\mu$ for $d = 1$ and 5 nm, respectively. (c) T_c as a function of $\bar{\mu}$ for various $\delta\mu$ and $d = 1$ nm. (d) T_c as a function of $\delta\mu$ for various $\bar{\mu}$ and $d = 1$ nm.

layers), there can, in principle, be inhomogeneous FFLO type solutions for the ground-state superfluidity in the system, but our general calculations allowing for the possibility of such inhomogeneous FFLO states fail to find any FFLO solutions for either the DMG or the DQBG systems, and we consistently find either purely homogeneous superfluid condensate or no condensate.

The interlayer screened interaction potential is calculated within the RPA, which is justfied for double layer graphene because the fermion number $N = 8$ is large, as

$$V(\mathbf{q},\omega) = \frac{v_q e^{-qd}}{1 + 2v_q (\Pi_u + \Pi_l) + v_q^2 \Pi_u \Pi_l (1 - e^{-2qd})}, \quad (2)$$

where $v_q = 2\pi e^2/(\epsilon q)$, Π_u and Π_l are the polarization functions for the upper and lower layers, respectively, and are functions of $\mathbf{q}$ and ω. The polarization functions are given for both the static ($\omega = 0$) limit and dynamic approximations in Ref. 21. The unscreened and static screening cases represent the two limits for the size of the gap in a real system: the unscreened interaction tends to overestimate the pairing and hence gives a large T_c, while the static screening tends to overestimate the screening efficiency and therefore yields a small T_c. In this article, we consider both these cases making the reasonable assumption that the reality of the situation is somewhere in-between.[12]

In the optimistic case of the unscreened interlayer Coulomb interaction, close layer separation ($d = 1$ nm), and a flat hBN substrate with $\epsilon = 3.9$, we find that T_c can be of the order of 100 K for realistic doping and moderate layer imbalance [see Fig. 1(a)]. As clarified in Fig. 1(c), T_c is a monotonically increasing function of $\bar{\mu}$, and larger $\delta\mu$ reduces T_c. Figure 1(d)
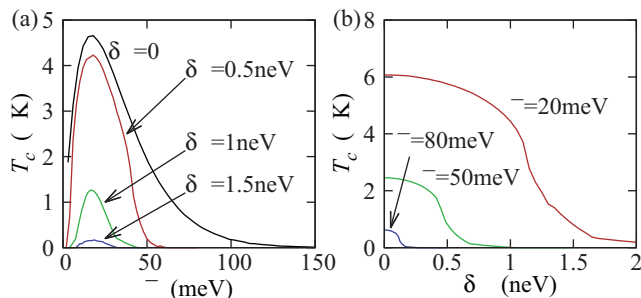
FIG. 2. (Color online) Static interlayer screening for DMG with $\Delta_{\mathbf{k}} = \Delta_{k_F}$. (a) For various $\delta\mu$ as a function of $\bar{\mu}$ and (b) for various $\bar{\mu}$ as a function of $\delta\mu$. Note that the scale on the vertical axis is micro-Kelvin.
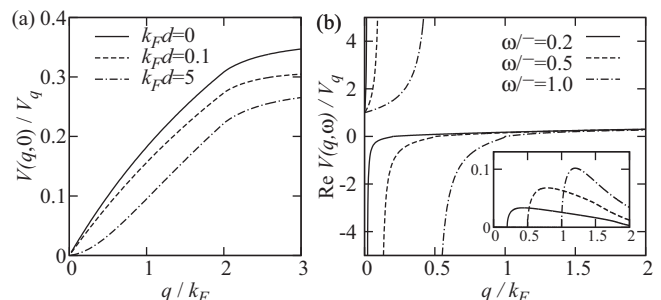

FIG. 3. Comparison of (a) the statically screened and (b) the real part of the dynamically screened interlayer interaction potentials to the unscreened interaction $V_q = 2\pi^2 e^{-qd}/(\epsilon q)$ for DMG with $\epsilon = 3.9$. The inset to (b) shows the imaginary part of the interaction.

shows that as the chemical potential asymmetry increases, T_c decreases monotonically with a characteristic "S" shape. Note that our theory neglects the possibility of direct tunneling between the layers, but this may become a significant factor and could even enhance the formation of the condensate[16] as the interlayer spacing becomes this small. Taking $d = 5$ nm, which is thick enough to fully suppress interlayer tunelling [see Fig. 1(b)], gives $T_c \approx 50$ K. We show our results in terms of $\bar{\mu}$ and $\delta\mu$ because these are the intuitive variables in the theory and allow for straightforward comparison with the results of the inhomogeneous case in Sec. II B. However, for experimental comparison, it is more convenient to parametrize in terms of carrier density than chemical potential. Straightforwardly, in the single-particle case, we have $\bar{n} = \bar{\mu}^2/(\pi\hbar^2 v_F^2)$, but δn depends nonlinearly on the fluctuation and the chemical potential as $\delta n = \delta\mu(2\bar{\mu} + \delta\mu)/(\pi\hbar^2 v_F^2)$.

We have repeated these calculations using the statically screened interlayer interaction finding that the gap is so small that our numerical procedure for T_c cannot resolve it within acceptable error bars. Therefore we suggest that the gap in this case is essentially zero even for $d = 1$ nm and $\epsilon = 1$. This happens because T_c is so small that the occupation factors, which appear in the self-consistent gap equation are very steep functions near the Fermi energy. Therefore, in order to produce a nonzero numerical result for Δ in this case, we approximated the gap as momentum independent. This is a reasonable approximation, also used, for example, in Ref. 14. Doing this yields the results shown in Fig. 2, which can be taken as a reliable upper bound on T_c with static screening. Figure 2(a) shows T_c as a function of $\bar{\mu}$ for several different values of $\delta\mu$, $\epsilon = 3.9$, and $d = 1$ nm. The behavior of T_c is qualitatively different from the unscreened case in that there is a maximal value of T_c, which depends sensitively on both ϵ and d. This is because as the carrier density increases, the screening becomes more effective and the interlayer interaction is reduced. To illustrate the dependence of T_c on $\delta\mu$, in Fig. 2(b) we show this for a few different values of $\bar{\mu}$. Notice that the scale on the horizontal axis is 10^{-9} eV, indicating that a tiny layer imbalance is enough to kill the condensate. However, the qualitative behavior of T_c with $\delta\mu$ is identical to the unscreened case.

To demonstrate why the statically screened interaction gives a T_c that is so low, in Fig. 3(a) we show as a function of momentum q the statically screened interaction

normalized by the unscreened potential $V_q = v_q e^{-qd}$. The potential is a universal function of q/k_F for $d = 0$, but is weakly dependent on $k_F d$ for finite d. We show representative curves for $k_F d = 0$, $k_F d \ll 1$, and $k_F d > 1$ corresponding to the strongest interaction limit, the low-density limit, and the high-density limit, respectively. We see that higher carrier density reduces the interaction strength since the increased density of states allows the screening to be more efficient. The static polarizability is constant up to $q = 2k_F$, but increases after that,[21] causing the noticeable flattening of the interaction potential as a function of q in Fig. 3(a). The peak of the gap function is found at $k = k_F$ and the most relevant contribution to the integrand in Eq. (1) comes from $k = k' \approx k_F$ indicating that the important range of wave vectors is $|q| < k_F$. In this regime, the statically screened potential is an order of magnitude smaller than the unscreened one leading to an excitonic gap, which is several orders of magnitude smaller than the unscreened case, consistent with previous analytical evaluations.[14]

The dynamically screened form of the interaction has been used by other authors, so we analyze the potential function (2) itself to gain some intuitive insight into the effect of this approximation. In Fig. 3(b), we show the dynamically screened interaction potential normalized by V_q as a function of wave vector for various frequencies and $k_F d = 0$. In this limit, the interaction is a universal function of q/k_F. The dynamic screening is a strong function of the frequency ω, however, some instructive patterns can be identified. For $q/k_F < \omega/\bar{\mu}$, the polarization functions are negative[21] and therefore it is possible for the finite frequency potential to have a divergence corresponding to the plasmon wave vector k_p. The potential also is negative[22] for $k_p/k_F < q/k_F < \omega/\bar{\mu}$ indicating an overall repulsive interaction which could reduce the gap size. In contrast, we note that for $q < k_p$, the interaction is enhanced over the unscreened case. This is the well-known antiscreening effect of dynamic screening, which should to some extent compensate for the sign change of the interaction in some regime of the phase space. For $q/k_F > \omega/\bar{\mu}$, the potential is very similar to the statically screened case. The most relevant frequency range is $\omega \approx \Delta$, which is in general rather small compared to $\bar{\mu}$ and hence the range of wave vectors where the potential deviates substantially from the statically screened case is small, indicating that T_c with dynamic screening will be closer to that predicted by the static screening calculation than

the unscreened one. This analysis also shows that a system with a large bare gap will be more robust against dynamic screening effects since the relevant frequency will be higher, implying that within the range of q that contributes strongly to the integrand in Eq. (1), we have $V(q,\omega)/V_q > 1$.

Calculations for the unscreened interaction for suspended DMG with $\epsilon = 1$ and $d = 1$ nm show that the excitonic gap is large with respect to $\bar{\mu}$ and therefore fluctuations of the order of the chemical potential will not reduce T_c to zero. When $d = 5$ nm, we find that T_c drops to room temperature or a little below. Suspended graphene is also known to form ripples with size fluctuations of the order of 1 nm in height,[23] which may make the precise control of the interlayer spacing difficult for these proposed devices, and which may introduce charge inhomogeneity related to the strain field induced by the corrugations. We shall discuss the effects of ripples in the next section, after we have described the role of charge inhomogeneity in DMG.

B. Charge inhomogeneity in DMG

In any experimental sample, some degree of extrinsic disorder-induced charge inhomogeneity will exist, as has been demonstrated by many surface measurements of monolayer graphene.[24–26] In a double layer device, the inhomogeneities in the charge landscapes will not be identical in both layers, and therefore there will be spatial variation in the asymmetry of the chemical potentials. In this situation, the local difference in chemical potential has two contributions. There is a nominally homogeneous part which is induced by gating and is, in principle, controllable. This contribution was the subject of the previous section and we ignore it here. Then there is a contribution from charged impurities and other disorder that is inhomogeneous and not controllable. A full analytical description of the inhomogenous system is clearly intractable so we employ an accurate numerical method to compute the charge density of the system when charged impurities explicitly break translational symmetry. From this charge landscape, we can assign the local chemical potential $\mu_u(\mathbf{r})$ and $\mu_l(\mathbf{r})$ in each layer, and characterize the spatial fluctuations by their root-mean square (rms) value, which is a measure of the typical fluctuation. Using this measure of the disorder in the charge landscape, we can discuss the stability of the condensate against the density and chemical potential inhomogeneity induced by the charged impurities. In principle, it is possible that some correlation will exist between charged impurities, although the nature of these correlations will depend on details of the system. We wish to avoid introducing extra parameters to describe this, so we assume uncorrelated disorder for the purposes of this work. If correlations are shown to be important, then they can be included within the theory we are about to describe in the same way as Ref. 27.

To calculate the charge landscape in each layer taking into account the presence of long-range disorder due to the charged impurities and nonlinear screening effects we use the TFDT.[19] The TFDT is a generalization to Dirac materials of the Thomas-Fermi theory.[28] TFDT and density-functional-theory (DFT)[29–32] are similar in spirit in the sense that they are both nonperturbative functional theories and therefore have the great advantage of being able to take into account nonlinear

screening effects that are dominant in systems like graphene at low doping. The key difference between TFDT and DFT in that in the latter, the kinetic energy operator is retained, while in the former it is replaced with a density functional. As a consequence, TFDT is computationally much more efficient than DFT and can be used to study large systems in the presence of long-range disorder where DFT is completely impractical. In particular, by using the TFDT, we are able to obtain disorder-averaged results which would be impossible with the strict DFT approach because of the heavy numerical cost. The simplified treatment of the kinetic energy term limits the validity of TFDT to regimes in which $|\nabla n/n| < k_F$. We have verified that this condition is reasonably well satisfied in single-layer graphene.[19,33] Our results show that in graphene double layers, due to the increased screening of the disorder potential caused by the presence of an additional graphene layer, the correlation length of the disorder-induced inhomogeneities is larger than in isolated single-layer graphene and therefore that the condition $|\nabla n/n| < k_F$ is always well satisfied in these double layer graphene heterostructures.

The carrier density in the ground state is obtained by minimizing the TFDT energy functional

$$
\begin{aligned}
E[n_u,n_l] = \; & E_u[n_u(\mathbf{r})] + E_l[n_l(\mathbf{r})] \\
& + \frac{e^2}{2\epsilon} \int d^2\mathbf{r} \int d^2\mathbf{r}' \frac{n_u(\mathbf{r})n_l(\mathbf{r}')}{(|\mathbf{r}-\mathbf{r}'|^2 + d^2)^{1/2}},
\end{aligned} \quad (3)
$$

where $E_i[n_i(\mathbf{r})]$ is the energy functional of the density profile for the ith graphene layer (as given in Ref. 19) and the last term is the interlayer Coulomb interaction. Each layer functional $E_i[n_i(\mathbf{r})]$ contains a term due to the disorder potential V_D created by the charged impurities. We also include intralayer exchange interactions. We assume that charged impurities located close to the surface of the SiO_2 constitute the dominant source of disorder and we therefore model the charged impurity distribution as an effective two-dimensional distribution $C(\mathbf{r})$ placed at a distance d_B below the lower graphene layer. Note that this is the most generous estimate for the charged impurities that we can take, since we are neglecting any disorder at the other interfaces which may be induced by the successive fabrication steps required to make these devices.[34] Denoting disorder-averaged quantities by angle brackets, without loss of generality, we assume $\langle C(\mathbf{r}) \rangle = 0$. We also assume the charged impurities to be uncorrelated[19,27,35] so that $\langle C(\mathbf{r})C(\mathbf{r}') \rangle = n_{\text{imp}}\delta(\mathbf{r} - \mathbf{r}')$, where n_{imp} is the charged impurity density. V_D in each layer is the Coulomb potential created by the random distribution $C(\mathbf{r})$. The ground-state density distributions $n_u(\mathbf{r})$ and $n_l(\mathbf{r})$ are obtained by minimizing $E[n_u,n_l]$ numerically enforcing the self-consistency of the distribution in the two layers due to the interlayer interaction. Then, the local difference in chemical potential between the two layers $\delta\mu_{\text{loc}} = \mu_u(\mathbf{r}) - \mu_l(\mathbf{r})$ can be extracted for each point in the system and by performing the minimization for many ($\sim$600) disorder realizations and we obtain statistics for the distribution function of $\delta\mu_{\text{loc}}$.

In Fig. 4, we show the spatial distribution of $\delta\mu_{\text{loc}}$ for three different impurity densities and in two experimentally relevant geometries. In the left column, we show data where the lower graphene layer is placed directly onto an SiO_2 substrate and the interlayer separation is $d = 1$ nm. In this case, the charged
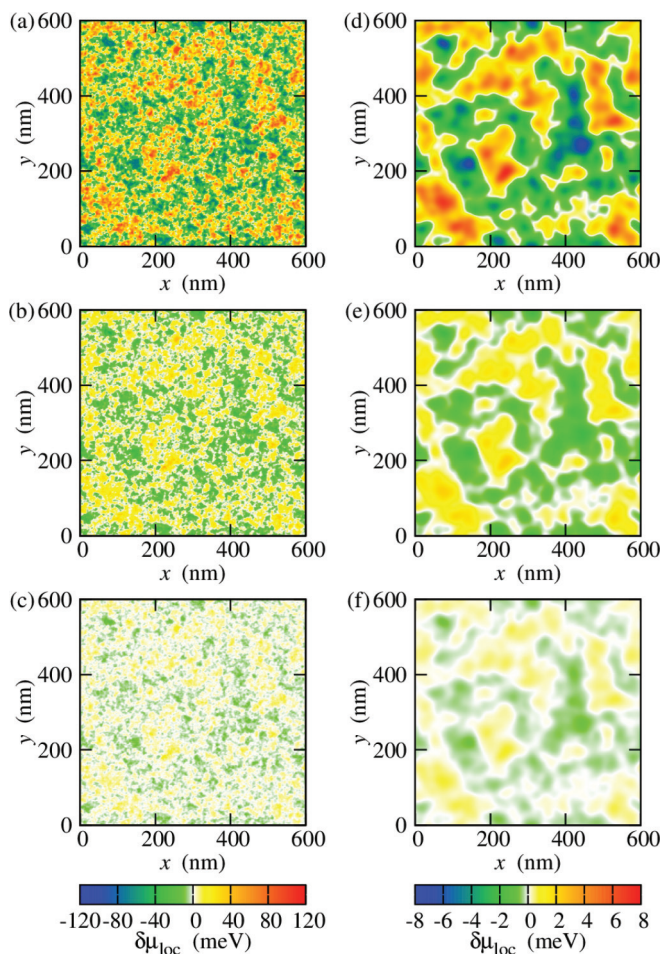
FIG. 4. (Color online) Spatial plots of $\delta\mu$ calculated via the TFDT. The left column is for $d = 1$ nm, $d_B = 1$ nm, and $\bar{\mu} = 50$ meV, which roughly approximates the experimental situation in Ref. 7. The right column is for $d = 5$ nm, $d_B = 20$ nm, and $\bar{\mu} = 200$ meV, which roughly approximates the experimental situation in Ref. 6. The color bar at the bottom of each column applies to all three plots in each column. The first row is for $n_{imp} = 10^{11}$ cm^{-2}, the second row is $n_{imp} = 10^{10}$ cm^{-2}, the third row is $n_{imp} = 10^9$ cm^{-2}.

impurities at the oxide interface are effectively approximated by a two-dimensional distribution 1 nm below the lower graphene layer, so we take $d_B = 1$ nm. This corresponds to the system used in the experiments in Ref. 7. We set $\bar{\mu} = 50$ meV corresponding to an easily achievable carrier density regime. The right column corresponds to a system where the lower graphene layer is seperated from the SiO$_2$ substrate by a 20 nm layer of hBN, like that used in the experiments in Ref. 6. Hence we take $d_B = 20$ nm, and we also set $\bar{\mu} = 200$ meV corresponding to the high carrier density regime where we expect the screening of the external impurities to be the most efficient, resulting in the lowest amount of charge inhomogeneity. In both situations, we assume that the gate-induced (homogeneous, controllable) part of the layer asymmetry to be zero. Therefore we assume that any layer imbalance is completely defined by the charged impurities. The rows of Fig. 4 show the data for, from top to bottom, $n_{imp} = 10^{11}$ cm^{-2}, 10^{10} cm^{-2}, and 10^9 cm^{-2}. (We note that the higher value of n_{imp} is more typical, and $n_{imp} = 10^9$ cm^{-2} is unlikely

to be achieved in laboratory graphene samples on any substrate. Typically, one can get an estimate of n_{imp} in a particular sample by looking at the carrier density regime over which the graphene minimum conductivity "plateau" exists around the Dirac point.[36]) All six plots share some similar qualitative features. In particular, they all show regions where $\delta\mu$ is positive and regions where it is negative with narrow strips in between where $\delta\mu$ is small.[37] The length scale of the fluctuations is not affected by the impurity density, but the magnitude of the fluctuations is. By comparing the data in the two columns, we see that the distance of the impurities from the DMG makes a substantial difference in the length scale of the fluctuations in $\delta\mu_{loc}$ and in reducing the magnitude of the fluctuations. The density of impurities also has a strong effect on the magnitude of the fluctuations in $\delta\mu_{loc}$ with the fluctuations reducing by approximately a factor of three with each order of magnitude decrease in n_{imp}. In the most dirty case (it should be noted that graphene on SiO$_2$ can have an impurity density of up to 5×10^{12} cm^{-2} as measured by transport measurements[36]), shown in Fig. 4(a) then the fluctutations in $\delta\mu_{loc}$ may be of the order of $\bar{\mu}$, indicating that the condensate has no opportunity to form in this case. For the cleanest situation shown in Fig. 4(f), the potential imbalance is on the scale of 1 meV and there is a significant chance that excitons with a gap of the size predicted by dynamic screening calculations[12] will persist in spite of the disorder if an impurity density as low as 10^9 cm^{-2} can be achieved in double layer graphene samples.

We take many disorder realizations ($\sim$600) for each impurity density and collect ensemble-averaged statistics for the distribution of $\delta\mu_{loc}$. We characterize this distribution by its root-mean-square value, which we label $\delta\mu_{rms}$. In Fig. 5, we plot $\delta\mu_{rms}$ for the two experimental geometries discussed above and for different interlayer spacing d. This is shown in Figs. 5(a) and 5(b) for $d = 1$ and 5 nm, respectively, for three impurity densities covering three orders of magnitude. The fluctuations are strongest at low carrier density, where the screening of the impurity potential is weakest, and it decreases monotonically with increasing $\bar{\mu}$. The trend suggested by the spatial plots is confirmed here, that is, decreasing the impurity density by a factor of ten generates approximately a factor of three reduction in the fluctuations. If the impurities are moved away from the DMG by a spacer layer as in Figs. 5(c) and 5(d), we find that the fluctuations in $\delta\mu$ are reduced to the order of 1 meV. This degree of fluctuation may be small enough to allow the condensate to be detected at a reasonable temperature scale. For the $d_B = 1$ nm case, a system dimension of 160-unit cells was chosen. For $d_B = 20$ nm, we increased that to 320 unit cells to ensure that the system was large enough to accurately capture the size of the typical fluctuations.

We briefly discuss the role of corrugations and ripples in the structure of the graphene lattice and describe their effect on the excitonic condensate. The existence of these ripples in suspended[23] samples and those placed on substrates of different kinds[26] have been demonstrated. In the case of suspended monolayer graphene, ripples of height of several angstroms have been observed,[23] indicating that a suspended double layer structure with small interlayer spacing may be difficult to control since ripple corrugations will then be of the same size as the layer separation. It has been theoretically
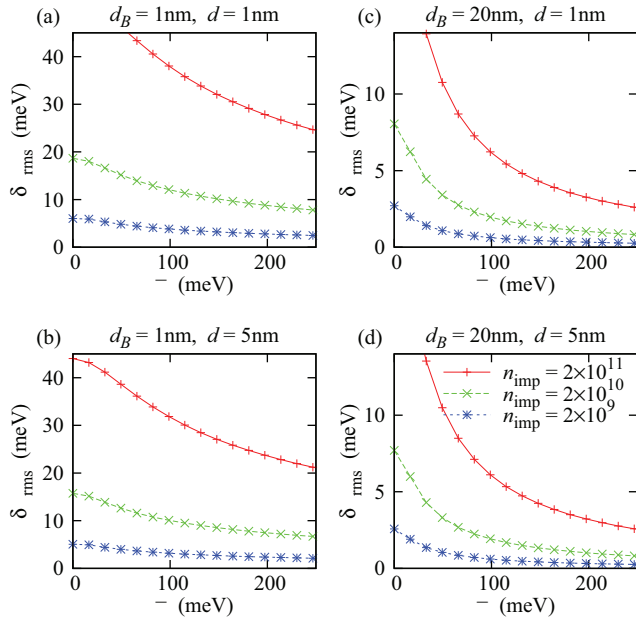
FIG. 5. (Color online) Root-mean-square of the distribution of the local $\delta\mu$ as a function of the global chemical potential for two experimentally relevant geometries. (a) and (b) $d_B = 1$ nm, $\epsilon = 3.9$ corresponding to double layer graphene placed straight onto a SiO$_2$ substrate per the experiments in Ref. 7. (c) and (d) $d_B = 20$ nm, $\epsilon = 3.9$ corresponding to double layer graphene placed onto a 20 nm slab of hBN per the experiments in Ref. 6.
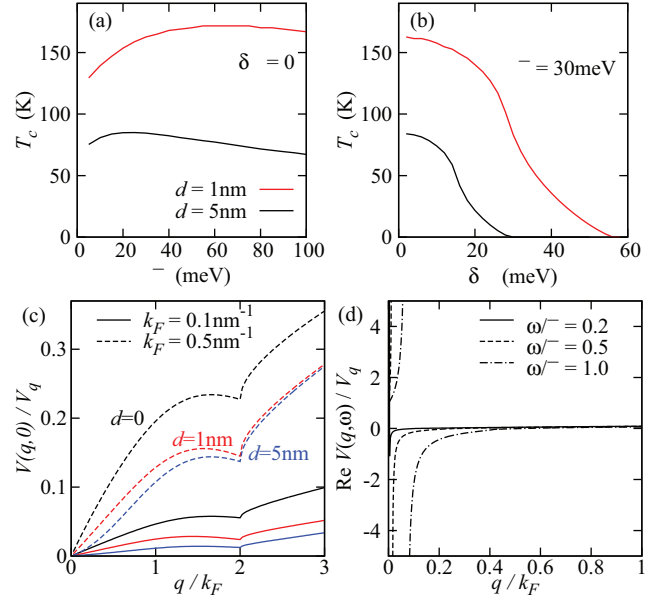

FIG. 6. (Color online) (a) T_c as a function of $\bar{\mu}$ with $\delta\mu = 0$ for double bilayer graphene with the unscreened interlayer interaction. (b) T_c as a function of $\delta\mu$ with $\bar{\mu} = 30$ meV. (c) The statically screened interlayer interaction for DQBG. (d) The dynamically screened interlayer interaction for DQBG in the high density regime ($k_F = 0.2$ nm^{-1}).

predicted[38–40] that the strain field associated with ripples can give rise to fluctuations in the local density of the order of 10^{12} cm^{-2}. If this is correct, then it shows that lattice corrugations may be a significant barrier to the existence of the condensate, since this will give $\delta\mu \approx 40$ meV, which would destroy the condensate even for unscreened Coulomb interactions.

III. DOUBLE BILAYER GRAPHENE

We now consider the analogous situation for double quadratic bilayer graphene (DQBG). In this case, two AB-stacked bilayer graphene sheets[41] replace the monolayers discussed previously. We employ the same approach as we did for DMG in that we analyze the critical temperature of the excitonic superfluid for the unscreened and statically screened interlayer interactions, and then examine the modification of the interlayer potential with the inclusion of dynamic screening effects. We model the two bilayer graphene sheets as having a gapless, quadratic low energy band structure $E_{\nu k} = \nu\hbar^2 k^2/(2m^*)$ where m^* is the effective mass which we assume to be the same in both layers, and $\nu = \pm 1$ denotes the band. Note that this approximation is only valid at densities $n < 3 \times 10^{12}$ cm^{-2}, which is approximately equivalent to $k_F = 0.3$ nm^{-1} and $\mu \approx 70$ meV. The difference in the low-energy band structure leads to qualitative changes in the behavior of the condensate as a function of $\bar{\mu}$, but not of $\delta\mu$, as we shall demonstrate. The gap equation in Eq. (1) and interlayer interaction in Eq. (2) are still valid in the double bilayer case, except for a redefined angular factor $f(\mathbf{k},\mathbf{k}') = \cos^2(\theta_k - \theta_{k'})/4$, exciton energy $E_{\mathbf{k}'} = [(\hbar^2 k'^2/(2m^*) - \bar{\mu})^2 + \Delta^2_{\mathbf{k}'}]^{1/2}$,

and the polarization screening function of the quadratic bilayer obviously needs to be taken into account.[42] Note that this is a similar system to that studied by quantum Monte Carlo methods recently,[43] where continuous transitions between a one-component fluid phase, an excitonic fluid phase, and a biexcitonic phase were predicted. However, that publication did not include any form of disorder.

We first show results for the unscreened interaction, using $V(q) = 2\pi e^2 e^{-qd}/(\epsilon q)$. In Fig. 6(a), we show T_c as a function of $\bar{\mu}$ and find that it is of the same order as for the equivalent case in DMG, i.e., $T_c \sim 100$ K for realistic interlayer separation [see Fig. 1(c)]. However, the nonmonotonicity of T_c as a function of overall density is unlike the monolayer case indicating that the interlayer separation and density of electrons have a more complex relationship than in the linear spectrum. This is due to the effective interaction parameter r_s being constant for monolayer graphene, but decreasing as $1/\sqrt{n}$ as a function of density for bilayer graphene. Therefore, as density increases, the reduced strength of the interactions in DQBG manifests as a smaller excitonic gap, thus reducing T_c. Figure 6(b) shows T_c as a function of $\delta\mu$ for $\bar{\mu} = 30$ meV. This shows qualitatively identical behavior as for DMG, indicating that within our BCS mean-field theory, the details of the underlying band structure do not qualitatively affect the response of the excitonic superfluid to asymmetrical layer doping. For comparison with experimental data where carrier density is a more useful variable, we note that for bilayer graphene in the single-particle limit that $\bar{n} = 2m^*\bar{\mu}/(\pi\hbar^2)$ and so the fluctuations are linear and $\delta n = 2m^*\delta\mu/(\pi\hbar^2)$.

As shown in Ref. 44, the static screening for quadratic bilayer graphene is somewhat stronger than for monolayer graphene, not just because the dimensionless polarizability is

larger, but because the density of states in the prefactor is also larger at low and moderate doping. This indicates that the interlayer interaction should be weaker in DQBG compared with DMG for comparable parameters. We find that the size of the gap is smaller than the accuracy of the numerical procedure that we employ. This indicates that, within our approximations for the statically screened interaction, T_c is expected to be smaller than a fraction of 1 nK. In contrast to the DMG case, the interlayer interaction $V(q,0)$ given in Eq. (2) is not a universal function of q/k_F for DQBG in the $k_F d = 0$ limit. Increasing the electronic density decreases the efficiency of the screening and allows the interlayer interaction to be stronger. This is a substantial qualitative difference between the screening in monolayer and bilayer graphene, which is understandable since quadratic bilayer has a constant density of states in contrast to the linear-in-energy density of states of monolayer graphene. The kink at $q = 2k_F$ corresponds to the $2k_F$ anomaly for $\Pi(q)$.[44] Also, increasing d will reduce the overall interaction strength which allows the screening to be more efficient, reducing $V(q,0)$ with respect to V_q, as in DMG.

For dynamic screening, we use previous results[42] for the finite frequency polarizability to determine the interaction potential. Figure 6(d) shows the dynamically screened interaction in the high density regime, where the interaction is the strongest. The high-q limit is the same as the static screening case, and we find that the dynamic screening reaches this limit even faster than in DMG. Therefore the interaction strength is weaker in DQBG and T_c is suppressed.

We now briefly comment on the role of inhomogeneity in DQBG. Since it is known that the response of the charge distribution to charged impurities in bilayer graphene is qualitatively similar to that in monolayer graphene,[19,45] it is very likely that the presence of charged impurities in the environment of the DQBG will have a similar detrimental effect on the stability of the condensate as for DMG. However, it is also known that bilayer graphene is, in general, somewhat more robust against ripples and corrogations than monolayer graphene,[46] indicating that charge inhomogeneity generated by this form of disorder may be slightly less important.

IV. CONCLUSION

In summary, we have presented a comprehensive analysis of the effect of charge inhomogeneity on T_c for the excitonic superfluid in double layer graphene systems. We find that the existence of charge inhomogeneity and ripples is likely to be the limiting factor for the stability of the condensate, but that the cleanest samples at low temperature should allow for the detection of the condensate. If the graphene layers are suspended, particular care must be taken to ensure minimal rippling since even in the absence of charged impurities, this may be a significant source of density inhomogeneity. We also investigated the equivalent situation in DQBG, showing that in the unscreened case, the quadratic nature of the low energy bands does change the qualitative behavior of T_c as a function of $\bar{\mu}$, but that the maximum achievable T_c is quite similar in both systems. However, static screening is somewhat stronger in DQBG but the details of the realistic screening are still unknown. Our most important conclusion is that the only
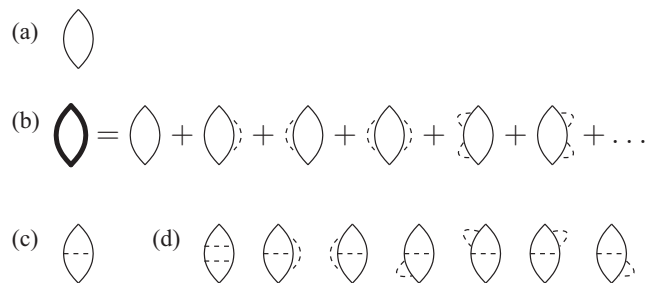

FIG. 7. (a) The diagram for $\Pi(\mathbf{q},\omega)$ in our calculation. (b) The diagram for $\Pi(\mathbf{q},\omega)$ in the calculation of Refs. 3 and 13. (c) The first-order diagram absent from (b). (d) The second-order diagrams absent from (b). The dashed lines represent interlayer electron-electron interactions.

hope for achieving excitonic condensation in graphene is to use very flat, ultrapure graphene with very low density of charged impurities so that the induced charge inhomogeneity is minimized. Even then, if the operative interlayer pairing interaction turns out to be the statically screened Coulomb interaction, there is very little hope for the observation of the interlayer superfluid state at any reasonable temperatures.

APPENDIX: SCREENING

In this Appendix, we clarify certain aspects of the screening models that are used both in the literature and in our own calculation. In particular, Refs. 3,12, and 13, use what the authors describe as a "self-consistent screening approximation." In this theory, the gap at the Fermi energy generated by the superfluid pairing is self-consistently included in the screening, with the result that the interlayer interaction is increased dramatically, enabling the condensate to be stable at temperatures of the order of 100 K. The fundamental issue we wish to raise is that the expansion of the polarization function on which these works rely does not include all diagrams of any arbitrary order in the electron-electron interaction. In Fig. 7(a), we show the zeroeth-order expansion, which we use in our calculation, and in Fig. 7(b) is the diagram and expansion to second-order used in Refs. 3 and 13. Figures 7(c) and 7(d) show, respectively, the first-order and second-order diagrams that are not present in this expansion. The absence of these diagrams violates the Ward identity for current conservation. As described in great detail in Refs. 47 and 48, the theoretical formulation of the dielectric response of a superconductor in the gapped symmetry-broken phase is a formidable task, which cannot be simulated simply by incorporating the self-energy in the polarization bubble diagram since such an approximation is not conserving as it leaves out many other diagrams (see Fig. 7 and Refs. 47 and 48) in each order. It is therefore theoretically more meaningful to use a clearly defined perturbative approach

where the screened interaction is calculated in the normal state (as done in the current paper) and then the BCS mean-field theory is carried out on this normal state interaction function. Our theory thus corresponds to the leading-order conserving perturbative approximation where only the bare bubble [see Fig. 7(a)] is used for the polarizability, thus satisfying the Ward identities. While this may not be a quantitatively accurate approximation, it is guaranteed to satisfy conservation laws. The inclusion of the vertex corrections to the ladder diagrams, which for the systems studied are not captured by the Migdal theorem, would be desirable but is well beyond the scope of this work (and, for that matter, all existing work in this subject) whose focus is the effect of long-range disorder on the conditions, in particular, T_c, for the realization of

excitonic superfluid states in DMG and DQBG. The issue of a better screening approximation going beyond RPA remains open for the graphene interlayer superfluidity problem since such a theory must combine the conserving approximation of Refs. 47 and 48 with the peculiar band structure and chirality of graphene physics.

In the current paper, we have demonstrated that DMG and DQBG have T_c of the same order for the equivalent level of approximation for the interlayer screening. How the consistent approximation of Refs. 47 and 48 would affect the excitonic condensation is currently unknown and remains an interesting open question, but it is not unreasonable to assume that the DMG and DQBG systems would still have T_c of the same order in this case.

---

[1] C.-H. Zhang and Y. N. Joglekar, Phys. Rev. B **77**, 233405 (2008).

[2] H. Min, R. Bistritzer, J.-J. Su, and A. H. MacDonald, Phys. Rev. B **78**, 121401 (2008).

[3] A. Perali, D. Neilson, and A. R. Hamilton, Phys. Rev. Lett. **110**, 146803 (2013).

[4] J. Zhang and E. Rossi, Phys. Rev. Lett. **111**, 086804 (2013).

[5] S. Banerjee, L. Register, E. Tutuc, D. Reddy, and A. MacDonald, IEEE Electron Device Lett. **30**, 158 (2009).

[6] R. V. Gorbachev, A. K. Geim, M. I. Katsnelson, K. S. Novoselov, T. Tudorovskiy, I. V. Grigorieva, A. H. MacDonald, S. V. Morozov, K. Watanabe, T. Taniguchi, and L. A. Ponomarenko, Nat. Phys. **8**, 896 (2012).

[7] S. Kim, I. Jo, J. Nah, Z. Yao, S. K. Banerjee, and E. Tutuc, Phys. Rev. B **83**, 161401 (2011).

[8] R. Bistritzer and A. H. MacDonald, Phys. Rev. Lett. **101**, 256406 (2008).

[9] D. K. Efimkin, V. A. Kalbachinskii, and Y. E. Lozovik, JETP Lett. **93**, 238 (2011).

[10] B. Dellabetta and M. J. Gilbert, J. Phys.: Condens. Matter **23**, 345302 (2011).

[11] D. S. L. Abergel, R. Sensarma, and S. Das Sarma, Phys. Rev. B **86**, 161412 (2012).

[12] I. Sodemann, D. A. Pesin, and A. H. MacDonald, Phys. Rev. B **85**, 195136 (2012).

[13] Y. E. Lozovik, S. L. Ogarkov, and A. A. Sokolik, Phys. Rev. B **86**, 045429 (2012).

[14] M. Y. Kharitonov and K. B. Efetov, Phys. Rev. B **78**, 241401 (2008).

[15] Y. E. Lozovik and A. A. Sokolik, JETP Lett. **87**, 61 (2008).

[16] M. P. Mink, H. T. C. Stoof, R. A. Duine, and A. H. MacDonald, Phys. Rev. B **84**, 155409 (2011).

[17] Y. E. Lozovik and V. I. Yudson, Sov. Phys. JETP **44**, 389 (1976).

[18] P. Pieri, D. Neilson, and G. C. Strinati, Phys. Rev. B **75**, 113301 (2007).

[19] E. Rossi and S. Das Sarma, Phys. Rev. Lett. **101**, 166803 (2008).

[20] C. Grimaldi, L. Pietronero, and S. Strässler, Phys. Rev. Lett. **75**, 1158 (1995).

[21] E. H. Hwang and S. Das Sarma, Phys. Rev. B **75**, 205418 (2007).

[22] Note that the overall negative sign for an attractive interaction is absorbed into the definition of the gap function in Eq. (1).

[23] R. Zan, C. Muryn, U. Bangert, P. Mattocks, P. Wincott, D. Vaughan, X. Li, L. Colombo, R. S. Ruoff, B. Hamilton, and K. S. Novoselov, Nanoscale **4**, 3065 (2012).

[24] J. Martin, N. Akerman, G. Ulbricht, T. Lohmann, J. H. Smet, K. von Klitzing, and A. Yacoby, Nat. Phys. **4**, 144 (2008).

[25] R. Decker, Y. Wang, V. W. Brar, W. Regan, H.-Z. Tsai, Q. Wu, W. Gannett, A. Zettl, and M. F. Crommie, Nano Lett. **11**, 2291 (2011).

[26] J. Xue, J. Sanchez-Yamagishi, D. Bulmash, P. Jacquod, A. Deshpande, K. Watanabe, T. Taniguchi, P. Jarillo-Herrero, and B. J. LeRoy, Nat. Mater. **10**, 282 (2011).

[27] Q. Li, E. H. Hwang, E. Rossi, and S. Das Sarma, Phys. Rev. Lett. **107**, 156601 (2011).

[28] G. F. Giuliani and G. Vignale, *Quantum Theory of the Electron Liquid* (Cambridge University Press, Cambridge, 2005).

[29] P. Hohenberg and W. Kohn, Phys. Rev. **136**, B864 (1964).

[30] W. Kohn and L. J. Sham, Phys. Rev. **140**, A1133 (1965).

[31] W. Kohn, Rev. Mod. Phys. **71**, 1253 (1999).

[32] M. Polini, A. Tomadin, R. Asgari, and A. H. MacDonald, Phys. Rev. B **78**, 115426 (2008).

[33] E. Rossi, S. Adam, and S. Das Sarma, Phys. Rev. B **79**, 245423 (2009).

[34] C. Dean, A. Young, L. Wang, I. Meric, G.-H. Lee, K. Watanabe, T. Taniguchi, K. Shepard, P. Kim, and J. Hone, Solid State Commun. **152**, 1275 (2012).

[35] Q. Li, E. Hwang, and E. Rossi, Solid State Commun. **152**, 1390 (2012).

[36] S. Das Sarma, S. Adam, E. H. Hwang, and E. Rossi, Rev. Mod. Phys. **83**, 407 (2011).

[37] It is possible that these strips with $\delta\mu \approx 0$ will allow the formation of percolating stripe states, but since our analysis of the BCS theory is not valid in this highly inhomogeneous regime, we do not examine it further.

[38] M. Gibertini, A. Tomadin, M. Polini, A. Fasolino, and M. I. Katsnelson, Phys. Rev. B **81**, 125437 (2010).

[39] P. Partovi-Azar, N. Nafari, and M. R. R. Tabar, Phys. Rev. B **83**, 165434 (2011).

[40] M. Gibertini, A. Tomadin, F. Guinea, M. I. Katsnelson, and M. Polini, Phys. Rev. B **85**, 201405 (2012).

[41] E. McCann and V. I. Fal'ko, Phys. Rev. Lett. **96**, 086805 (2006).

[42] R. Sensarma, E. H. Hwang, and S. Das Sarma, Phys. Rev. B **82**, 195428 (2010).

[43]R. Maezono, P. López Ríos, T. Ogawa, and R. J. Needs, Phys. Rev. Lett. **110**, 216407 (2013).

[44]E. H. Hwang and S. Das Sarma, Phys. Rev. Lett. **101**, 156802 (2008).

[45]E. Rossi and S. Das Sarma, Phys. Rev. Lett. **107**, 155502 (2011).

[46]X. Chang, Y. Ge, and J. M. Dong, Eur. Phys. J. B **78**, 103 (2010).

[47]H. A. Fertig and S. Das Sarma, Phys. Rev. Lett. **65**, 1482 (1990).

[48]H. A. Fertig and S. Das Sarma, Phys. Rev. B **44**, 4480 (1991).